Available online at www.sciencedirect.com
ScienceDirect
Earth and Planetary Science Letters 263 (2007) 104–113
EPSL
www.elsevier.com/locate/epsl

High resolution imaging in the inhomogeneous crust with cosmic-ray muon radiography: The density structure below the volcanic crater floor of Mt. Asama, Japan

Hiroyuki K.M. Tanaka [a,b,c,*], Toshiyuki Nakano [d], Satoru Takahashi [d], Jyunya Yoshida [d], Minoru Takeo [a], Jun Oikawa [a], Takao Ohminato [a], Yosuke Aoki [a], Etsuro Koyama [a], Hiroshi Tsuji [a], Kimio Niwa [d]

[a] *Earthquake Research Institute (ERI), University of Tokyo, 1-1-1 Yayoi, Bunkyo, Tokyo 113-0032, Japan*
[b] *Atomic Physics Laboratory, RIKEN, 2-1 Hirosawa, Wako, Saitama 351-0198, Japan*
[c] *Physics Department, University of California, Riverside, CA 92521, USA*
[d] *Physics Department, Nagoya University, Furo-cho, Chikusa, Nagoya, Aichi 464-8602, Japan*

Received 7 May 2007; received in revised form 3 September 2007; accepted 3 September 2007
Available online 8 September 2007
Editor: C.P. Jaupart

Abstract

We have developed a novel radiographic imaging method to survey the inhomogeneous structure of the crust. As an example, we performed measurements at Mt. Asama volcano, and studied the feasibility of using an azimuthally isotropic flux of cosmic-ray muons in the energy range up to a few TeV. The principle of the technique is that by measuring muon absorption along different nearly horizontal paths through a solid body, one can deduce the density distribution in the interior of the object. A muon detector with an area of 4000 cm^2 was installed in a 1-m deep instrument vault located about 1 km from the summit crater of Mt. Asama. Muon tracks within emulsion layers in the detector were analyzed by 3d image processing to determine the level of energy absorption along different ray paths through the summit crater region. A typical angular resolution of the muon detector of 10 milliradians (mrad) corresponds to a spatial resolution of 10 m at a distance of 1 km. The measurements would be ideal for studying the shallow structure of the crust at sites which cannot be well resolved because of their strong structural heterogeneity and potential difficulty to be accessed, and which therefore cannot have their structure determined by conventional electromagnetic or seismic techniques. The present method can also provide three dimensional images of the subsurface by making measurements from two or more different points. In this work, we have radiographically imaged a few hundred meters below the crater floor of Mt. Asama, Japan, and have detected a dense region, which corresponds to the position and shape of a lava mound created during the last eruption (Urabe, B., Watanabe, N., Murakami, M., Topographic change of the summit crater of Asama Volcano during the 2004 eruption derived from Airborne Synthetic Aperture Radar (SAR) measurements, Bulletin of Geographical Survey Institute, 53, 1–6 (2006).). Right below the lava mound we found a low density region that suggests a drain-back-induced porous conduit (Urabe, B., Watanabe, N., Murakami, M., Topographic change of the summit crater of Asama Volcano during the 2004 eruption derived from Airborne Synthetic Aperture Radar (SAR) measurements, Bulletin of Geographical Survey Institute, 53, 1–6 (2006).). The density contrast was resolved with a precision of 1–3%. This method

* Corresponding author. Earthquake Research Institute (ERI), University of Tokyo, 1-1-1 Yayoi, Bunkyo, Tokyo 113-0032, Japan.
E-mail address: ht@riken.jp (H.K.M. Tanaka).

0012-821X/$ - see front matter
doi:10.1016/j.epsl.2007.09.001

provides a resolution of the shallow density structure that is significantly higher than is possible with conventional geophysical measurements.

Keywords: cosmic-ray muon; radiography; emulsion cloud chamber; volcano; vulcanian eruption

1. Introduction

The internal structure of the Earth's crust is commonly studied by seismological, electromagnetical or gravitational geophysical observations. However, these measurements are rather indirect and have substantial intrinsic uncertainties. Therefore it is desirable to find independent ways to assess subsurface structure in order to reduce these ambiguities. Among the measured properties of the Earth's interior, density plays a special role because it is most readily interpreted in terms of composition and state. These could represent local-scale geological processes, such as the movements of magma in the conduit of a volcano. Thus, independent measurements of density would be of considerable value. Here we discuss a novel way to image the density distribution in the shallow crust, by providing a cosmic-ray radiograph of Mt. Asama volcano, as an example.

Cosmic-ray muons are particles generated in the atmosphere that continuously bombard the Earth's surface from above. They arrive at angles ranging from vertical to horizontal (Thompson et al., 1975) with an extremely small number of neutrino-induced muons directed upward. These particles are highly penetrating and a typical horizontally-arriving cosmic-ray muon with an energy of 1 TeV penetrates 2.6 km of water. Thus, cosmic-ray muon radiography can be applied to km-size objects located at elevations above where the detector is placed. Cosmic-ray muon radiography is similar to X-ray radiography, except penetrating muons serve in place of X-rays. In cosmic-ray muon radiography, a detector with a small area ($\sim m^2$) is placed at a shallow depth underground with the aim of imaging a volume that is higher in elevation adjacent to the detector. The intensity of an image pixel in the detector is determined by the attenuation of incident muons caused by absorption in the Earth's crust. This technique is utterly independent of the geophysical model, and directly measures the density length (density × path length). By determining the path lengths from topographic information, the measurement gives us the average density $<\rho>$ along the path lines of cosmic-ray muons through the Earth. The energy loss of muons through matter can be calculated by exploiting relations in the Standard Model of muon-initiated interactions which is sufficiently well known for the purpose of radiography (Particle Data Group, 1998; Adair and Kasha, 1976; Groom, 2001). The uncertainty due to theory in these calculations is small. By measuring the muon absorption rate we can detect a small change in $<\rho>$ due to the existence of either less-dense or more-dense areas inside. The method can be remotely operated. Standard geophysical methods require to be operated on site. This can be difficult due to field conditions, or dangerous due to the volcanic activity. The required observation time is inversely proportional to the area of the detector used. For example, the time required for resolving a 3% change in $<\rho>$ in 1 km of rock is 2 months with a 1000 -cm^2 detector at solid angle intervals of 0.01 steradians (sr).[1] Several groups have tried to use this method to see inside a pyramid (Alvarez, 1970; Maya Muon Tomography) and beneath volcanoes (Tanaka et al., 2003; Tanaka et al., 2005; Tanaka et al., 2007).

Recent developments of the particle detector using an emulsion cloud chamber (ECC) (Nakamura et al., 2006) have motivated this radiographic study of a volcano using a position sensitive detector designed to detect the particle tracks of cosmic-ray muons with an angular error of a few mrad in the emulsion layers. Furthermore, the ECC detector is a completely power-free particle tracking device and is light enough to be carried up to a mountain. The method can be remotely operated. Standard geophysical methods require to be operated on site. This can be difficult due to field conditions, or dangerous due to the volcanic activity. In this paper, we describe the procedure we used to map the density contrast of the crust using cosmic-ray muon radiography, we present a novel view below the crater floor of Mt. Asama with an image resolution significantly higher than it is possible with conventional geophysical measurements.

2. Cosmic-ray muon sources

Radiography using the propagation of muons uses a well known energy spectrum for muons arriving at different zenith angles, a well understood muon detector, and a specific muon propagation model through matter. If the Earth structure along the muon path is unknown, the

[1] The steradian (sr) is the SI unit of solid angle.

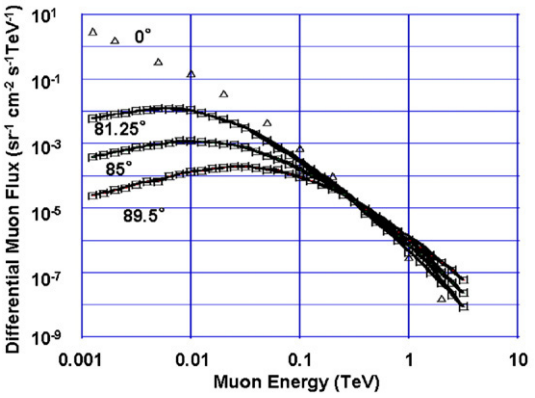

Fig. 1. Energy spectrum of cosmic-ray muons for different zenith angles, where the experimental data are from DEIS (Allkofer et al., 1981) and the curves are the results of the model calculation for large angles.

information from counting muon events in the detector at different arriving angles can be used to infer the properties of the matter through which the muons travelled.

Interactions of very high energy cosmic-rays with the atmosphere produce a flux of high energy cosmic-ray muons, and their energy spectrum is well known (Allkofer et al., 1981). These muons come mostly from the vertical, following a known zenith angular distribution. It is also well known that muons are arriving in the horizontal direction with a smaller average intensity, but with a higher intensity at energies above a few 100 GeV. Because muons become highly penetrative as their energy becomes higher, these horizontal muons can be used for the purpose of radiography of the shallow crust. Since the muon flux is reasonably high, the size of the detector that is required is reasonable for geologic applications. Fig. 1 shows the muon energy spectrum for different zenith angles. At large angles, low energy muons decay before they interact, thus the average muon energy increases. Solid lines show theoretical curves (Thompson et al., 1975) for large arriving angles.

The way in which high energy muons are stopped when travelling through matter has been studied well and is summarized in various articles (Particle Data Group, 1998; Adair and Kasha, 1976; Groom, 2001). The energy loss of a charged particle of energy E in tera electron volts (TeV) through matter with a density length of X hectograms per cm^2 (hg/cm^2)[2] can be written as (Adair and Kasha, 1976):

$$dE/dX = a + bE \quad (1)$$

where the first term represents the ionization loss and the second term represents various stochastic processes.

[2] A density length of 1hg/cm^2 is equivalent to 1m of water (m.w.e).

Table 1
Muon range R and energy loss parameters calculated for standard rock

E_μ (GeV)	R (km.w.e)	a (MeV g^{-1} cm^2)	b (MeV g^{-1} cm^2)
10	0.05	2.15	1.91
100	0.41	2.40	3.12
1000	2.42	2.58	4.01
10,000	6.30	2.76	4.40

Range is given in km-water-equivalent.

Table 1 shows a and b values for standard rock (mass number=22, proton number=11, density=2.65 g/cm^3) as a function of muon energy. Because the muons interact with electrons and nucleons, the attenuation is directly proportional to the density of the material with minimal uncertainty due to chemical composition. Only the integrated effect along the travel path leads to attenuation of flux. Then, once the density length (X) along the path is determined the minimum energy (E_c) of the cosmic-ray muons which can penetrate through this distance is determined by Eq. (1). By integrating from E_c to infinity we obtain the integrated muon events $N_\mu(E_c, \theta^*)$, the number of muons which have enough energy to escape from the area of interest. Inversely, for a substance with unknown X, a measurement of the muon flux $N_\mu(E_c, \theta^*)$ uniquely determines its density length, X. Absolute density value measurements have been performed using vertical cosmic-ray muons (Crouch, 1987; Andreev et al., 1987; Ambrosio et al., 1995). Fig. 2 shows the vertical muon intensity versus depth in units of km of water equivalent (km.w.e). Fig. 3 shows the integrated flux of cosmic-ray muons, $N_\mu(E_c, \theta^*)$ at various zenith angles penetrating through a given thickness of rock, X, in units of km of water equivalent.

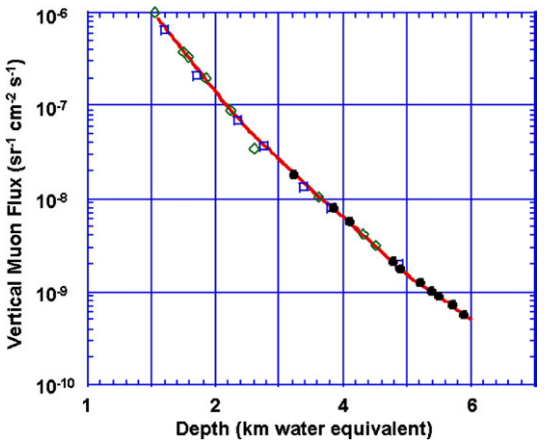

Fig. 2. Vertical muon intensity versus depth (1 km.w.e. of standard rock). The experimental data are from ◇: the compilation of Crouch (1987), □: Baksan (Andreev et al., 1987), ●: MACRO (Ambrosio et al., 1995).

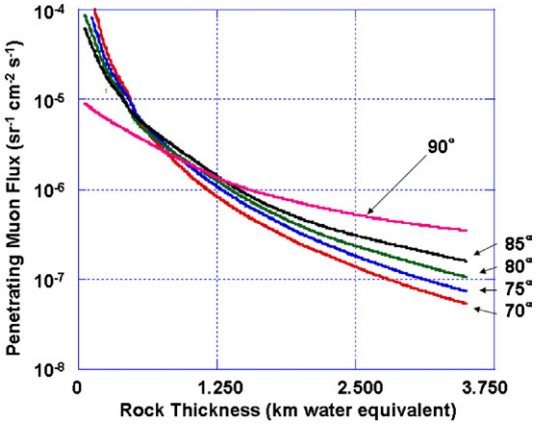

Fig. 3. Integrated flux of cosmic-ray muons at various zenith angles penetrating through a given thickness of rock with a density of 2.5 g/cm^3.

2.1. Muon detectors

In order to test the feasibility of the proposed method, we deployed an emulsion cloud chamber (ECC) for the detection of horizontal cosmic-ray muons passing through Mt. Asama. Mt. Asama, is one of the most active andesitic volcanoes in Japan and last erupted on September 1, 2004. The summit elevation is 2560 m above sea level, and the size of the crater is 350 m in diameter and ~200 m deep (Fig. 4) (Topographical map, 2004, 2005, 2006). In 2004, GSI (Geographical Survey Institute, Japan) measured geomorphic changes of the crater floor using Airborne Synthetic Aperture Radar (AirSAR). The results indicated a pancake shaped lava mound had formed on the crater floor during the 2004 eruption (Urabe et al., 2006). The image of the SAR is generated using the results of distance measurement between the radar source and the terrain surface. Thus, the crater wall causes a shadow area on the image where no signals come back from the terrain.

This emulsion cloud chamber (ECC) detector that was used to perform cosmic-ray muon radiography at Mt. Asama had a relatively large detection area (4000 cm^2) and with a high precession in angular determination. This ECC detector was designed to measure the incoming charged particle flux. Micro-crystals of AgBr are incorporated in the emulsion layers of the detector. When a fast charged particle passes through this layer, part of the micro-crystals on the particle trajectory records the path and these paths can be analyzed when the emulsion is later developed, somewhat like photographic film. The space required for the entire setup (40 cm length × 50 cm wide × 10 cm thickness × 2 sets) was reasonable for our test experiment.

Initial radiography investigations with the ECC detector at Mt. Asama used a smaller detection area (700 cm^2) and its angular resolution, detection accuracy and performance were evaluated by imaging the external shape (the surface) of the mountain and the upper most region of the main crater (Tanaka et al., 2007). Unexpected charged particles can also be recorded in

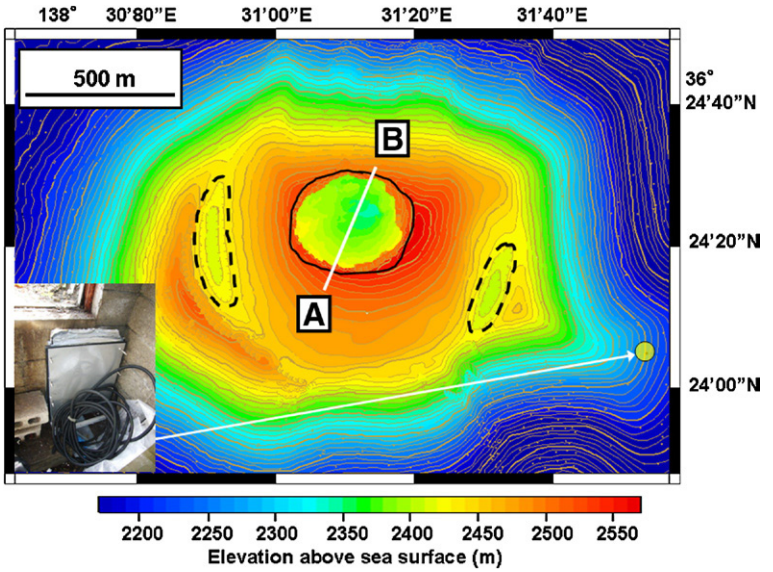

Fig. 4. Map of Mt. Asama showing the location of the cosmic-ray muon detector (arrow). Inset is a photograph showing the emulsion-cloud-chamber cosmic-ray muon detector made of iron plates and nuclear emulsion films. The white solid line A–B, parallel to the horizontal edge of the detector, shows the vertical cross-sectional plane of the crater in Fig. 6. The old crater (dotted black lines) of Mt. Maekake-yama has been buried with a new pyroclastic cone (Mt. Kama-yama) with a summit crater (solid black line).

the emulsion layers and become a serious source of background noise. The reduction of such background noise not only saves time during particle detection analysis but also provides much finer precision. This problem was solved by placing the detector underground in a vault (at an elevation of 2250 m) where other geophysical instruments are placed (the inset of Fig. 5). The geometrical arrangement used in the present measurement is shown in Fig. 5. The muon flux arriving from the backward direction, mainly transmitted through air can be used to confirm whether or not the muon flux recorded in the ECC detector is azimuthally isotropic at the observation point. Since cosmic-ray muons do not arrive from the downward direction, we can distinguish "forward-directed" from "backward-directed" muon trails by choosing either positive ($+\theta$) or negative arriving angles ($-\theta$), as shown in Fig. 5.

The data processing methods for the ECC data are described in detail elsewhere (Tanaka et al., 2007; Nakamura et al., 2006) and only briefly described here. Tracks from the emulsion films were digitized and read into a computer. sixteen tomographic CCD images are read through a microscope in the 45 micron thick emulsion layers, and tracks in these images are recorded in three dimensions by an image processor.

2.2. Analysis

In the reconstructing procedure, various muon paths are analyzed. Because the size of the ECC detector is much smaller than the object of interest (the volcanic conduit), the path of each muon can be represented by an azimuth and a zenith angle with reference to a line perpendicular to the detector plane (θ, ϕ; $\theta = 90° - \theta^*$). The histogram obtained of the number of events, N_μ as a function of (θ, ϕ) can be normalized by the cosmic-ray muons not passing through the volcano (those from the backward direction). In the present case, the muons at $\theta > 440$ mrad (25.2°) arrive directly from the sky (Fig. 5). We call this value the *observed attenuation factor* ($f_o(\theta, \phi)$).

Using the conventional cosmic-ray muon absorption rate through matter, we estimated the average density of the lava mound formed on the crater floor during the 2004 eruption using Monte-Carlo particle tracking simulation as follows. First, we defined the geometry of the summit crater from the 1/25,000 topographic map distributed by GSI (Topographical map, 2004, 2005, 2006). Throughout this work standard physical processes, as indicated by Eq. (1) were used in GEANT4 (Agostinelli et al., 2003) to compute the energy loss when high energy muons are stopped when travelling through the volcano. In order to simulate the cosmic muon flux, each muon is treated as an individual beam that is generated in front of the detector with a randomised incident angle. The muon momentum spectrum is based on the measurements of the muon flux (Fig. 1) with a cut off for energies below 1 GeV. Simulation of the incident angle distribution was generated with a minimum angular deviation from vertical set to 60°. If the distance between the point where the muon enters the volcano and the point at which the energy of the muon becomes zero is longer than the

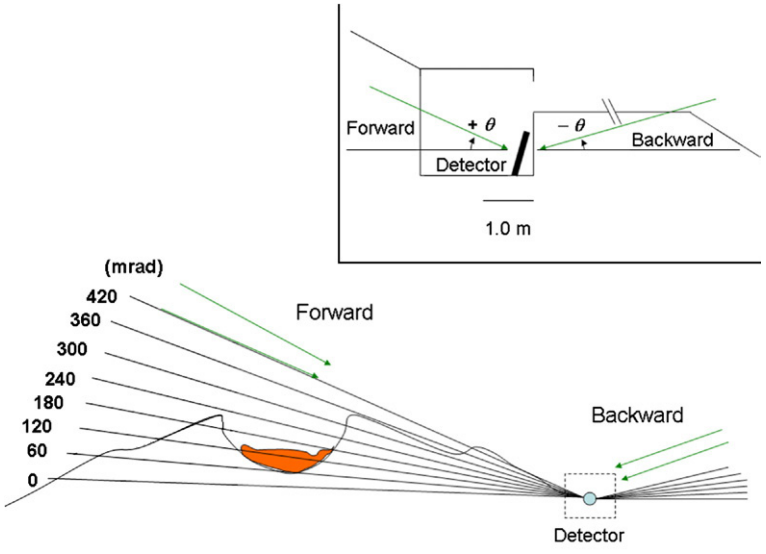

Fig. 5. Cross-section of Mt. Asama showing geometrical arrangements used in the present measurements. The data for muons arriving from the backward direction are also used to confirm the detector efficiency. The inset shows the detector arrangements in the underground space.

density length, the zenith and azimuth angles of the muon track are written to a data file. The averaged density length $\rho = X/L(\theta, \phi)$ can be calculated by reading a topographic map.

The *simulated transmission factor* ($f_s(\theta, \phi, \rho)$: the number of muons passing through the volcano as a function of the vertical angle (θ), azimuth angle (ϕ), and the average density (ρ) along the path can be computed as

$$f_s(\theta, \phi, \rho) = N_\mu(\theta, \phi, \rho)/N_\mu(\theta, \phi, 0) \quad (2)$$

We start by assuming a trial density profile, our initial guess of the *simulated transmission factor* $f_s(\theta, \phi, \rho)$ for the object (in the present case, Mt. Asama) as a function of vertical and azimuth angle (θ, ϕ) and the trial density (ρ_{trial}). Initially this density profile is defined as a uniform density distribution. The *simulated transmission factor* based on this profile is then compared with the observed transmission factor $f_o(\theta, \phi)$, the angular distribution of the observed flux integrated over energy. By minimizing $\chi^2(f(\phi))$, the best fit gives the optimized *simulated transmission factor* for the average density over the azimuth angles ($\rho_{trial} -> \rho_{averaged}$). The points that deviate from the fitted curve are recognized as anomalies. From the amount of deviations we correct the attenuation factor according to Eq. (2). Again this is compared with the *observed transmission factor*. The *simulated transmission factor*, $f_s(\theta, \phi, \rho_{trial})$ can then be further improved by using the modified value of the density profile. This procedure is repeated until convergence is obtained for the difference between the simulated and observed angular distribution of the muon flux ($\rho_{averaged} -> \rho_{optimized}$).

3. Results and discussion

The radiographic image (Fig. 6), plotted as the *observed transmission factor* ($f_o(\theta, \phi)$) above the elevation where the detector was placed, is effectively a cross section through the volcano parallel to the plane of the detector, on which the average density along all the muon paths is projected. For Mt. Asama, this image shows two relatively high transmission factor ($f_o(\theta, \phi) > 10^{-3}$) zones (the yellow and green zones in Fig. 6-a), one at the left and the other at the centre. The zone at the left corresponds to the part of the old crater of Mt. Maekake which was activated about 8500 years ago, and the shadow at the centre corresponds to the present main crater of Mt. Asama. The weaker (or stronger) muon transmissions come from: a longer (shorter) path length and a higher (lower) average density along the path. From the raw attenuation factor projection (Fig. 6), two strong density–length anomalies are observed. One is due to long path (position $(\theta, \phi) = (150–310, 30–290)$ and $(620–780, 30–230)$), the other due to high density (position $(\theta, \phi) = (300–600, 50–180)$). The muons arriving from the backward direction are also reduced below $\theta < 150$ mrad because they are absorbed in the overlying soil. The muons arriving from the backward directions (mainly transmitted through air) are also plotted in the same angular region in Fig. 6.

The discussion is now focused on the central anomaly. First, the high attenuation region coincides with the position and shape of the lava mound emplaced in the 2003 crater floor during the 2004 eruption (between white and black dashed lines in Fig. 6-a) with dense lava. Second we found a low density region below, that we interpret as the drain-back of lava in the conduit. This drain-back mechanism is consistent with the intermittent collapses of the crater floor that occurred between 22 October 2004 and 11 January 2006 (Urabe et al., 2006). This structure can be clearly seen in the average density mapping shown in Fig. 7-a with a vertical spatial resolution of ±30 m and a horizontal resolution of ±60 m. From the density distribution projection (Fig. 7), a low density (blue) zone is observed below the high density (red) region at position $(\theta, \phi) = (400–540, 30–50)$. The way this density map is obtained from the attenuation map is described in Section 2. The thickness of the lava mound shown in Fig. 7-a has been reconstructed from Airborne SAR scanning of the crater floor surface (performed on 11 January 2006) (Urabe et al., 2006). The region that we cannot estimate the topography from the SAR measurement is indicated in Figs. 6 and 7 as “radar shadow zones”. Our interpretation of the low density region is that the drain-back process created a porous magma supply path below the crater floor. After the eruption ended, the collapse of the crater floor began, presumably reflecting lava drain-back. As shown in Fig. 6, there exists a sufficient number of comics-ray muons which penetrate the rock through a thickness of 1.0–1.5 km, demonstrating that cosmic-ray muon radiography is a viable technique to observe the internal structure of the crust on such a spatial scale.

In our radiographic measurements, we have confirmed the following important properties of the present method, which will be useful for future geophysical measurements:

(1) With 2 months of observations, an average density determination within a thickness of a few hundred meters can be made with an accuracy of 1–2%

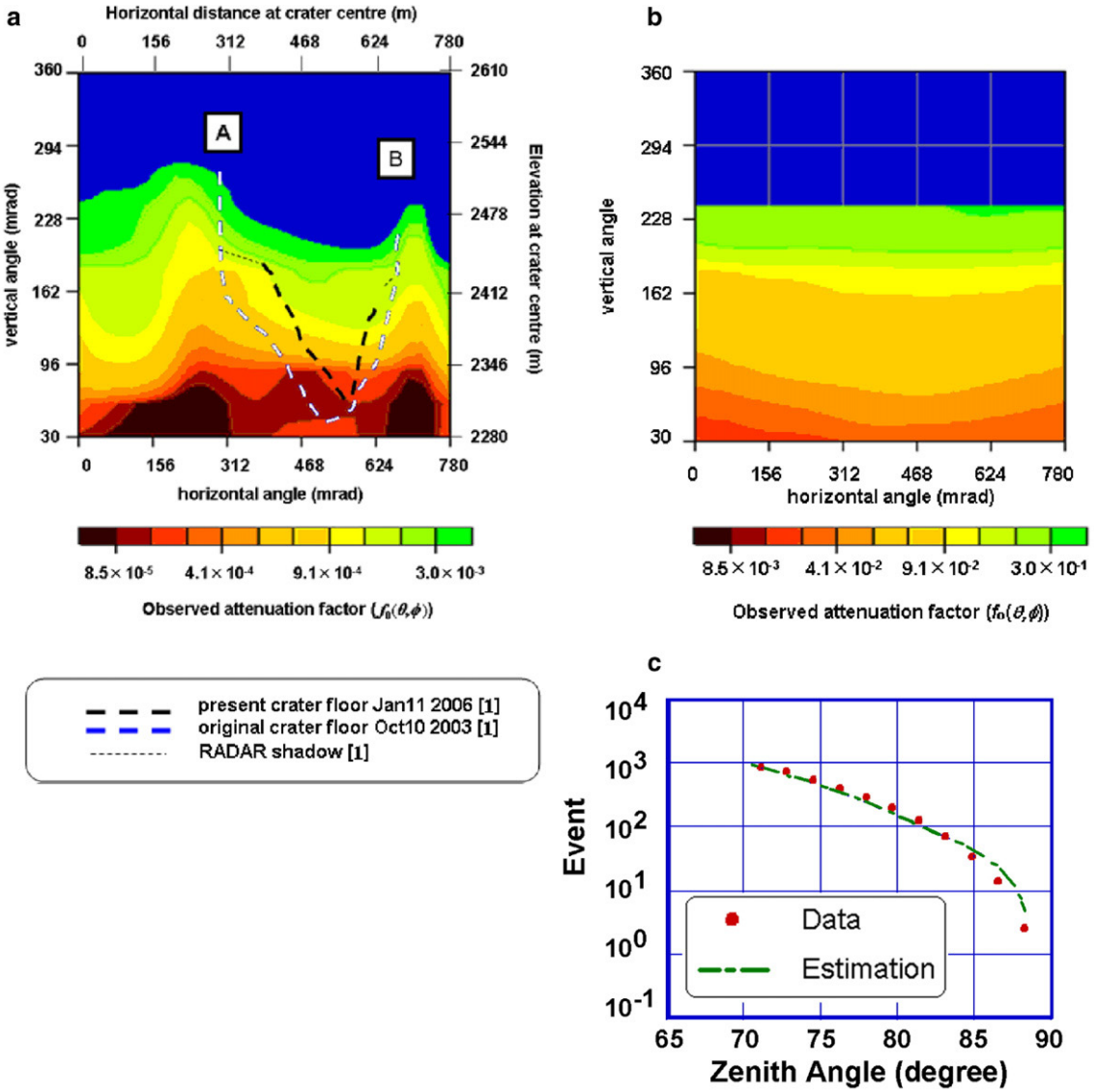

Fig. 6. (a) Radiographic image of the summit region of Mt. Asama, (b) the image as plotted using the backward muon data, and (c) the comparison of the zenith-angle dependence of the total muon count with the numerically estimated angular dependence. The region above the elevation where the detector was placed is plotted. The position and the shape of the 2003 and the 2005 craters shown on the map of Mt. Asama (Fig. 4) are overlaid on this plot. The bottom and the left axes indicate the horizontal and vertical arriving angles (θ, ϕ in units of mrad) with reference to the line perpendicular to the detector plane. The top and right axes are in units of meters corresponding to the horizontal distance and the elevation at the centre of the crater. The radiographic image is plotted as the *observed transmission factor* ($f_o(\theta, \phi)$). The weaker (or stronger) muon transmissions come from: (1) a longer (shorter) path length and (2) a higher (lower) average density along the path.

and with a vertical resolution of ±30 m and a horizontal resolution of ±60 m at 1.0 km distance. The spatial resolution and density contrast of the internal structure that is resolved depends on the number of detected muons that pass through the region or feature of interest, and thus they can be improved simply by using a larger detector. Fig. 7-b summarizes the tradeoff between observation time and density contrast for features to be resolved to within one standard deviation with the present ECC detector (4000 cm^2). In order to constrain the density variations below the crater floor with 1 week of observations, we need about 100 muon events from the region of interest. This is potentially achievable using a detector with a size of 2 m × 2 m.

(2) These kinds of measurements can be easily carried out by placing ECC detectors at the foot of a mountain. Electricity is not necessary because the detector is passive and requires no power. The cost

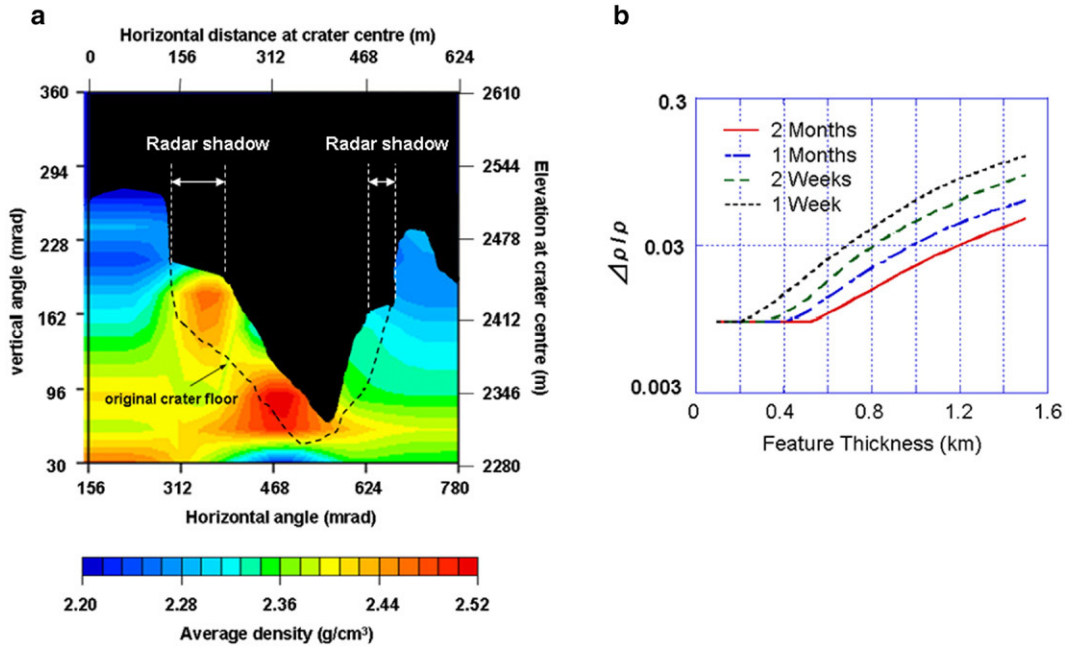

Fig. 7. (a) Reconstructed average density distribution for each muon path line and (b) the number of muons required to resolve, to one standard deviation, the presence of a feature of given thickness and differential density with respect to surrounding material with the present experimental setup. The average density distribution is plotted projected on the cross sectional plane. The distribution of the average density was reconstructed by applying the range-energy relationship for cosmic-ray muons through rock to the path length (L) calculated from the surface shape of the mountain for each arriving angle.

required for all the equipment and the space needed for accommodating the entire setup are both reasonable. The method does not require to go on site, while other geophysical methods need onsite measurements.

(3) Assuming the stronger muon absorption found in the 2003 crater is only due to the lava mound, the average density ($<\rho>$) map (Fig. 7) shows that $<\rho>$ along the muon path lines through the lava region is about 5% higher than that through the surrounding area at the same depth. We found that the bulk density of the lava mound is 2.76–2.84 g/cm^3, and the radiographically determined surrounding density of 2.27–2.33 g/cm^3, taking into consideration that the ratio of the path length between the lava mound and the surrounding rock is $\sim$0.2. This value is typical for andesitic lava.

(4) We found the lower density region right below the 2003 crater floor (the blue patch observed at the bottom in Fig. 7). The reliability of blue patch observed at the bottom (Fig. 7) was evaluated by considering following two factors: (a) the value of the experimental error, and (b) accuracy of the topographic map. The value of the experimental error (2.5% in determining the density length) was evaluated from the azimuthal distribution of the backward muon intensity (Tanaka et al., 2007). The errors raised by the path length estimation using the topographic map (1/25,000) (Topographical map, 2004, 2005, 2006) may in some cases be as high as 30 m compared to the 1500 m path length. This would be 2.0%. Therefore, the total density length relative error becomes 3.2%, which is smaller than the difference in $<\rho>$ between the blue patch and the surrounding area. Assuming this region is cylindrically-symmetric about the vertical axis, with a diameter of 150$\pm$60 m (where the error corresponds to the horizontal resolution of the image, discussed above), we found that the bulk density of this low-density region is 0.8$\pm$0.2 g/cm^3. This value corresponds to a bulk porosity of 25–45%, suggesting a very high permeability. If there is a permeable region right below the vent cap (the lava mound) volcanic gases can move freely within this zone, and might be stored and confined in this region during future events.

(5) In general, bulk density increases with depth, as shown in Fig. 7, reflecting compression by the overlying soil. Seismic velocity structure can be compared with such independently obtained information on the density distribution.

(6) The radiographic image shows that the volcanic conduit is now sealed at the top by the large mass of the vent cap, consistent with models of vulcanian eruptions (Self et al., 1979). Exsolved volatiles and vaporized

ground water may be confined below this lava cap before the next eruption. Therefore, this technique might provide a way to forecast a volcanic eruption by monitoring changes in the density along the magma channel inside the summit region of a volcano. Obviously this would depend on the time scale which density changes occurred at the volcano, how often the measurements were made, and how long it takes to analyze the results. A new sensor, called a scintillator could be a candidate for this purpose. Scintillators convert a muon's energy to light when a high energy muon passes through them. The light can be detected by photo sensors such as photomultiplier tubes. By processing the signal from photomultipliers using high speed electronic circuits, a real-time application could be possible.

4. Conclusions

Horizontally arriving cosmic-ray muons can be used to explore the internal structure of the shallow inhomogeneous crust, such as at a volcano. We have performed a radiographic survey at Mt. Asama to confirm the feasibility of this method and found two important results. First, we show evidence that the 2003 crater is covered by the dense lava mound that was erupted in 2004 and which functions as a vent cap. Second, we infer the existence of a porous and permeable region below the cap. This technique can be applied to any type of geological feature above the elevation where the detector is located. The measurement yields information on anomalies in the density distribution, such as from dense lava, a low density magma supply path or the compression with depth of the overlying soil. The detection method described here is relatively simple and inexpensive and provides information for geologic interpretations of various near surface phenomena. The limitation of this method includes: (a) it is limited to near-surface depths and strongly depends on the nature of the local topography (the detector must be placed on a slope pointing toward a topographically prominent feature of interest, and there will only be results for the volume located above the detector); (b) the method is limited to horizontal ranges of 2–3 km (which limits the potential targets).

We anticipate our technique to be a starting point for more in situ monitoring of volcanic activities. This technique only resolves the average density distribution along individual muon paths. Therefore, the user must end up making assumptions or interpretations about more localized structure along those muon paths, or must use more than one detector to resolve the three-dimensional density structure. This is why volcanoes make good study targets because they are axi-symmetric and it is reasonable to assume that the observed density variations are localized in the vent or crater area. However, this uncertainty could be further constrained with multiple observations from two or more cosmic-ray muon detectors. They would serve two important purposes: they could reduce the time required to obtain density measurements with reduced statistical and systematic errors, and also could provide three-dimensional structure below the volcanic surface. Furthermore, time-dependent cosmic-ray radiography could detect changes with time making it suitable for real-time monitoring applications, possibly providing evidence of precursor activity. Such a technique could also be applied to any other geological features on the Earth. Further research is required to improve the ability to detect, interpret and understand subsurface crustal structure, and to reduce measurement uncertainties. The success of these cosmic-ray muon observations will motivate the next level of collaboration between particle physics and geophysics.

Acknowledgements

The authors are deeply indebted to K. Kodama of Aichi University of Education and M. Komatsu of Nagoya University for their valuable contributions. Special funding arrangements by S. Okubo and related people of ERI and JSPS (Japanese Society of Promotion of Science) are acknowledged. H. Watanabe and T. Koyaguchi of ERI and K. Nagamine of UCR are also acknowledged for their valuable suggestions. This work greatly benefited from useful comments by William Chadwick and a reviewer of this manuscript.

References

Adair, R.K., Kasha, H., 1976. In: Hughes, V.W., Wu, C.S. (Eds.), Muon Physics, vol. 1. Academic Press, p. 323.

Agostinelli, S., et al., 2003. Geant4: a simulation tool kit. Nucl. Instrum. Methods A 506, 250–303.

Allkofer, C.O., et al., 1981. Muon Spectra from DEIS up to 7 TeV, Proc. of 17th Cosmic Ray Conf. (Paris), 10, p. 321.

Alvarez, L.W., 1970. Search for hidden chambers in the pyramids. Science 167, 832–839.

Ambrosio, M., et al., 1995. (MACRO collaboration), vertical muon intensity measured with MACRO at the Gran Sasso laboratory. Phys. Rev. D52, 3793–3802.

Andreev, Yu.M., Gurentzov, V.I., Kogai, I.M., 1987. Proc. 20th Int. Cosmic Ray Conf. (Moscow), 6, p. 200.

Crouch, M., 1987. Proc. 20th Int. Cosmic Ray Conf. (Moscow), 6, p. 165.

Groom, D.E., 2001. Muon stopping power and range tables 10 MeV–100 TeV. At. Data Nucl. Data Tables 78, 183–356.

Maya Muon Tomography at University of Texas at Austin High Energy Physics Labs web page http://www.hep.u-texas.edu/mayamuon/.

Nakamura, T., et al., 2006. The OPERA film: new nuclear emulsion for large-scale, high-precision experiments. Nucl. Instrum. Methods A 556, 80–86.

Particle Data Group, 1998. Review of particle physics. Eur. Phys. J. C 3, 1–794.

Self, S., Wilson, L., Nairn, I., 1979. Vulcanian eruption mechanisms. Nature 277, 440–443.

Tanaka, H., Nagamine, K., Kawamura, N., Nakamura, S.N., Ishida, K., Shimomura, K., 2003. Development of a two-fold segmented detection system for near horizontally cosmic-ray muons to probe the internal structure of a volcano. Nucl. Instrum. Methods A 507, 657–669.

Tanaka, H.K.M., Nagamine, K., Nakamura, S.N., Ishida, K., 2005. Radiographic measurement of the internal structure of Mt. West Iwate with near-horizontal cosmic-ray muons and future developments. Nucl. Instrum. Methods A 555, 164–172.

Tanaka, H.K.M., Nakano, T., Takahashi, S., Niwa, K., 2007. Development of an emulsion imaging system for cosmic-ray muon radiography to explore the internal structure of a volcano, Mt. Asama. Nucl. Instrum. Methods A 575, 489–497.

Thompson, M.G., et al., 1975. The production spectra of the parents of vertical cosmic ray muons. J. Phys. G: Nucl. Phys. 1, L48–L50.

Topographic map distributed by Geographical Survey Institute Japan 2004–2006.

Urabe, B., Watanabe, N., Murakami, M., 2006. Topographic change of the summit crater of Asama Volcano during the 2004 eruption derived from Airborne Synthetic Aperture Radar (SAR) measurements. Bulletin of Geographical Survey Institute 53, 1–6.